Available online at www.sciencedirect.com
ScienceDirect
Polyhedron 26 (2007) 4719–4730
POLYHEDRON
www.elsevier.com/locate/poly

A new ruthenium nitrosyl species based on a pendant-arm 1,4,8,11-tetraazacyclotetradecane (cyclam) derivative: An experimental and theoretical study

Ariel G. De Candia, Juan P. Marcolongo, Leonardo D. Slep *

Departamento de Química Inorgánica, Analítica y Química Física, INQUIMAE, Facultad de Ciencias Exactas y Naturales Universidad de Buenos Aires, Pabellón 2, Ciudad Universitaria, C1428EHA Buenos Aires, Argentina

Received 3 February 2007; accepted 26 April 2007
Available online 10 May 2007

Abstract

The complex *cis*-$[Ru(L^{py})NO]^{3+}$ (**I**) (L^{py} = *N*-(2-methylpyridyl)1,4,8,11-tetraazacyclotetradecane) was prepared by the stoichiometric reaction between $Ru(dmso)_4Cl_2$ and L^{py} and an excess of $NaNO_2$ in ethanolic medium, followed by acidification of the solution. The diamagnetic species was isolated as its hexafluorophosphate salt, and fully characterized by IR ($\nu_{NO} = 1917\ cm^{-1}$) and diverse NMR techniques in combination with theoretical computations based on the density functional theory (DFT). The compound displays strong electronic transitions below 300 nm and weak ones in the visible region of the spectrum, all of them solvent insensitive. The reaction of *cis*-$[Ru(L^{py})NO]^{3+}$ with OH^- generates the strongly colored nitro compound *cis*-$[Ru(L^{py})NO_2]^+$ (**II**) The $\{RuNO\}^6$ compound can be interconverted into the one-electron reduced $\{RuNO\}^7$ species *cis*-$[Ru(L^{py})NO]^{2+}$ (**III**). The reduction process is completely reversible in the cyclic voltammetry timescale with E^0 (versus Ag/AgCl, 3 M Cl^-) = −0.02 V and 0.18 V in water and acetonitrile, respectively. Controlled potential reduction in both solvents yields to the quantitative formation of **III**, a process which involves significant changes in the electronic spectroscopy. The $\{RuNO\}^7$ species proved to be inert against ligand loss, and electrogenerated solutions remained unchanged for several hours if protected from atmospheric oxygen. Electrochemical reoxidation or exposure to air lead to the complete recovery of the starting *cis*-$[Ru(L^{py})NO]^{3+}$ material, without signs of secondary reactions. The robustness of the coordination sphere appears as a consequence of the multidentate nature of L^{py}.

Keywords: Nitrosyl; Ruthenium; Redox conversion; Electronic structure; Spectroscopy

1. Introduction

Metal nitrosyl complexes have been known for quite a long time, and a considerable amount of well characterized nitrosyl compounds that cover different coordination numbers has been reported [1,2]. The overall structural and reactivity features of metal nitrosyls has been classically rationalized in terms of their $\{MNO\}^n$ description, where *n* stands for total number of metal d- and nitrosyl π^*-electrons [3]. This description avoids any mention to the identity of the ligand environment, which basically does not influence the most significant geometrical features (M–NO angle) within complexes of a given $\{MNO\}^n$ configuration. However, it is known that the first coordination sphere may exert a significant impact on the spectroscopic and reactivity properties: it determines the values for the redox potentials of the metallonitrosyl couples ($E_{MNO^+/MNO}$) and strongly influences the electrophilic reactivity of $\{MNO\}^6$ species [4–10]. One-electron reduction of an $\{MNO\}^6$ species is the typical route employed to access the $n = 7$ oxidation level [7,9,11]. The structural and spectroscopic characterization of these complexes with $n = 7$ has been thoroughly achieved in the recent years [8,12–14]. However their reactivity properties still remain poorly investigated.

* Corresponding author. Tel.: +54 11 4576 3380x110; fax: +54 11 4576 3341.
E-mail address: slep@qi.fcen.uba.ar (L.D. Slep).

0277-5387/$ - see front matter © 2007 Elsevier Ltd. All rights reserved.
doi:10.1016/j.poly.2007.04.038

We are currently interested in studying the reaction of $\{MNO\}^7$ complexes with dioxygen in aqueous medium, a study with both fundamental and bioinorganic relevance. Recent reports [11,15] suggest that the rate constant of this process (k_{ox}) might be significantly influenced by the redox potential of the $E_{MNO^+/MNO}$ couple, leading to a linear free-energy relation (LFER) between ln k_{ox} and $E_{NO^+/NO}$ with a negative slope value close to the one predicted by the Marcus model. This result has been rationalized in terms of an associative mechanism that involves the formation of a covalent bond between molecular oxygen and the $\{MNO\}^7$ moiety [15]. Complementary, this same study suggests that six-coordination is crucial to achieve fast oxidation of bound $NO^{\cdot}$ and NO^- complexes, but certainly a more systematic investigation of the autoxidation reaction of hexacoordinated $\{MNO\}^6$ species appears as necessary.

In spite of the large amount of well-described species of this kind, it is not an easy task to find literature examples of water-soluble nitrosyl species with robust coordination spheres that remain unaffected upon redox changes [16]. Examples with the appropriate redox potential to explore their reactions with dioxygen are even scarcer. We explore here one possible alternative to obtain such a species, namely the use of pendant-arm derivatized *N*-macrocyclic ligands. We report the preparation, isolation and characterization of the $\{RuNO\}^6$ species *cis*-$[Ru(L^{py})NO](PF_6)_3$ (**I**) (L^{py} = *N*-(2-methylpyridyl) 1,4,8,11-tetraazacyclotetradecane), focusing on its electronic structure an the possibility of redox interconversion to the one-electron reduced $\{RuNO\}^7$ species.

2. Experimental

2.1. Materials and reagents

The reagents employed in the synthetic procedures were purchased to Aldrich or Merck, and were used without further purification. All the organic solvents employed in synthetic procedures or physical determinations were dried and freshly distilled before used, following standard procedures. The precursor complex $Ru(dmso)_4Cl_2$ [17] and the ligand *N*-(2-methylpyridyl) 1,4,8,11-tetraazacyclotetradecane [18] were synthesized according to previously published procedures. A vacuum line and Schlenk glassware were employed when the manipulations required exclusion of air.

2.2. Synthesis of $[Ru(L^{py})NO](PF_6)_3$ (*I*)

One hundred and seventy milligrams (0.35 mmols) of $Ru(dmso)_4Cl_2$ where added to 35 mL of an ethanolic solution of 102.6 mg of L^{py} (0.35 mmol) under argon. The solution was refluxed for 4 h, reaching a deep orange color. The mixture was allowed to cool down to room temperature. 0.50 g (7.2 mmol) of $NaNO_2$ were added to the reaction mixture, which was further refluxed for 5 h. After cooling down, the reaction mixture was treated with 6.5 mL of HCl 6 M, and the volume reduced to a few mL by vacuum distillation. Addition of 5 mL of a saturated water solution of NH_4PF_6 induced the precipitation of 300 mg of a brownish microcrystalline powder. Recrystallization of this solid by diffusion of diethyl ether into an acetonitrile solution yielded 155 mg (52%) of analytically pure **I**, as revealed by elemental analysis and ^1H and ^{13}C NMR spectroscopy. *Anal.* Calc. for $C_{16}H_{29}F_{18}N_6OP_3Ru$: C, 22.4; H, 3.4; N, 9.8. Found: C, 22.2; H, 3.6; N, 9.7%. ν_{NO} (KBr) = 1917 cm^{-1}. δ_H (CD_3CN): Aromatic protons, 8.59 (1H, d), 8.36 (1H, t), 7.89 (1H, d), 7.85 (1H, t). Amine protons, 9.70 (1H), 9.33 (1H), 6.91 (1H) observed as broad signals. Aliphatic protons, 5.10 (1H, d), 4.88 (1H, d), 3.83 (1H), 3.72 (3H), 3.38 (1H), 3.31 (4H), 3.18 (1H), 3.09 (1H), 2.99 (1H), 2.89 (1H), 2.77 (1H), 2.54 (1H), 2.37 (1H), 2.33 (1H), 2.23 (1H) partially obscured by the solvent, 2.09 (1H), 2.02 (1H). The multiplicity of the signals is not given due to the complexity of the coupling pattern. See text for a detailed discussion. δ_C (CD_3CN): Aromatic carbons, 161.8, 153.9, 144.9, 128.1, 124.9. Aliphatic carbons, 73.6, 65.2, 60.0, 58.2, 56.2, 54.0, 51.0, 50.7, 48.1, 26.6, 23.3.

2.3. Physical measurements

Microanalytical data for C, H, N and O were obtained at INQUIMAE, with a Carlo Erba EA 1108 analyzer. UV–Vis spectra were recorded with either an HP8453 or an HP8452A diode array spectrometer. IR spectral measurements were carried out using alternatively one of two FT spectrophotometers, a Nicolet 150P and a Thermo Nicolet AVATAR 320. Spectra were collected from KBr disks. NMR data were acquired on a Bruker AM500 spectrometer operating at 500.13 MHz for ^1H. Standard pulse sequences were used for two-dimensional (2D) heteronuclear single quantum coherence (HSQC), correlated spectroscopy (COSY) and nuclear Overhauser enhancement spectroscopy (NOESY). Cyclic voltammetry (CV) and square wave voltammetry (SWV) measurements were done in aqueous 0.1 M $HClO_4$ or in organic medium (0.1 M Bu_4NPF_6 as supporting electrolyte) with a standard three electrode cell [19] containing a Pt working electrode (1.5 mm ∅) or a vitreous carbon electrode (3 mm ∅), and a Pt wire as a counterelectrode. As a reference in aqueous media, a commercial Ag/AgCl (BAS) electrode was used. In organic medium, a Ag wire and ferrocene as internal standard was used [20]. Throughout this work, all the reported redox potentials are referred to Ag/AgCl, 3 M NaCl (0.21 V versus NHE). The potential of the working electrode was controlled with one of two commercial potentiostats (Princeton Applied Research 273A or TEQ-03). The spectroelectrochemical experiments in the UV–Vis region were done in a homemade cell containing a quartz cuvette (1 cm path). The potential was controlled with a TEQ-03 potentiostat, using either 0.1 M $HClO_4$ or 0.1 M Bu_4NPF_6 in acetonitrile as supporting electrolyte. A commercial Ag/AgCl reference electrode was used in

aqueous solution whereas a $Ag/AgNO_3$ (0.01 M Ag^+ in acetonitrile) electrode was the reference employed in organic medium. The working and counter electrodes were a Pt net and a Pt wire, respectively. The system was maintained at 25 ± 0.1 °C for the experiments in water and at -30 ± 1 °C for those in acetonitrile (RC6 LAUDA thermostat), and was entirely purged with N_2. In a typical experiment, the solution was electrolyzed at sufficiently low potential (*ca.* 200 mV below the E^0 values registered by CV) in several cathodic steps. Between consecutive reduction periods, the solution was allowed to equilibrate and the open-circuit potential (E_{oc}) together with the UV–Vis spectrum were recorded. Redox potentials and disclosed UV–Vis spectra of the reduced and oxidized species were then obtained by global analysis [21]. This procedure involves a simultaneous multi-wavelength fitting to the Nernst equation [22].

2.4. Theoretical calculations

We employed density functional theory (DFT) computations to fully optimize the geometries of the cations $[Ru(L^{py})NO]^{3+}$, $[Ru(L^{py})NO]^{2+}$, $[Ru(L^{py})NO_2]^{+}$ and $[Ru(L^{py})Cl]^{+}$ in vacuo, without symmetry constraints. The calculations were performed with *Gaussian 03* [23], at the B3LYP level, employing the LanL2DZ basis set, which proved to be suitable for geometry predictions in coordination compounds containing metals of the second and third raw of the transition elements in the Periodic Table [11,24]. We used tight SCF convergence criteria and default settings in the geometry optimizations. Depending on the case (see text below) several minima along the potential energy surface were explored by scanning one particular internal coordinate. The true nature of all the found stationary points, which correspond to (local) minima in the potential energy surface were confirmed by numerical vibrational frequency computations. In all cases the absence of negative frequencies confirmed that the optimized geometries correspond to stable configurations in the potential energy surfaces. Time dependent (TD)DFT computations at the equilibrium geometry were employed as an assistant tool in the interpretation and assignment of the electronic spectra.

3. Results and discussion

3.1. Synthetic strategy and structural characterization of $[Ru(L^{py})NO]^{3+}$

Mono *N*-substitution of 1,4,8,11-tetraazacyclotetradecane (cyclam) can be performed under controlled reaction conditions, employing a large excess of cyclam with respect to the alkylating agent [18,25]. *N*-(2-methylpyridyl) cyclam (L^{py}) is therefore prepared in good yield by the reaction of 2-(chloromethyl)pyridine and a large excess of cyclam in DMF. Separation of the product from the unreacted macrocycle can be easily achieved because of the notoriously different solubility properties of both species. The pentadentate ligand is conveniently incorporated into the coordination sphere of Ru(II) by reaction with $Ru(dmso)_4Cl_2$ in ethanol in the absence of oxygen. This process seems to yield a mixture of products (most probably $[Ru(L^{py})Cl]^{+}$, $[Ru(L^{py})dmso]^{2+}$ and $[Ru(L^{py})(solv)]^{n+}$) that are difficult to isolate and purify. Nevertheless, the reaction of this mixture with nitrite leads to the formation of the nitro derivative $[Ru(L^{py})NO_2]^{+}$. Acidification of the reaction mixture induces acid–base changes in the coordinated ligand as in Eq. (1) [5,26–28], and yields the desired $\{RuNO\}^6$ core.

$$[Ru(L^{py})NO_2]^{+} + 2H^{+} \rightleftarrows [Ru(L^{py})NO]^{3+} + H_2O \quad (1)$$

The ^1H NMR spectrum of **I** in CD_3CN (Supplementary material) consists of 29 partially or totally overlapped signals that also show extensive scalar coupling. This spectrum is a consequence of the rigidity of the macrocycle combined with the lack of symmetry elements, which makes all protons non-equivalent. The ^1H NMR resonances at 8.59, 8.36, 7.89 and 7.85 ppm, referred to as H_{18}, H_{20}, H_{21} and H_{19}, respectively (see Fig. 1 for proton numbering), can be safely ascribed to the pyridine moiety by comparison with the free ligand. Note that complex **I** can potentially present isomerism leading to *cis*- or *trans*-species. However, the observation of a single set of signals for the aromatic protons seems to be consistent with the occurrence of a single isomer.

The three broad features at 9.70, 9.33 and 6.91 ppm, not observed when the spectrum is recorded in D_2O solution, can be attributed to the three exchangeable N*H* protons. The pyridine linker methylene N–CH_2-py protons give rise to two doublets at 4.88 and 5.10 ppm, coupled by one large $^2J(HH) \approx 17.5$ Hz. The remaining features in the range between 2 and 4 ppm, can be altogether assigned to the geminal pairs of CH_2 protons in the cyclam backbone. The ^{13}C NMR spectrum in CD_3CN, shows signals from each one of the 16 macrocyclic ligand carbon atoms (Supplementary material).

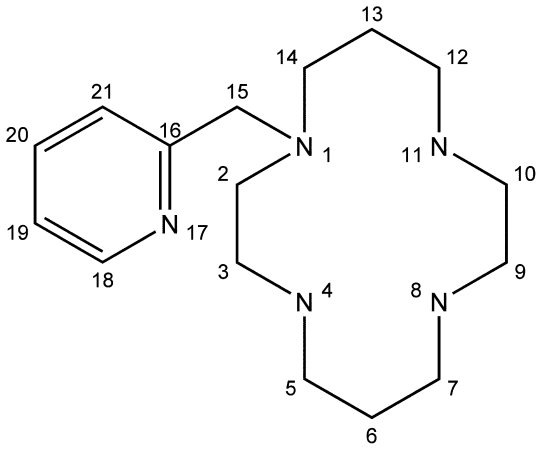

Fig. 1. Atom numbering used to identify the nuclei in the NMR discussion.

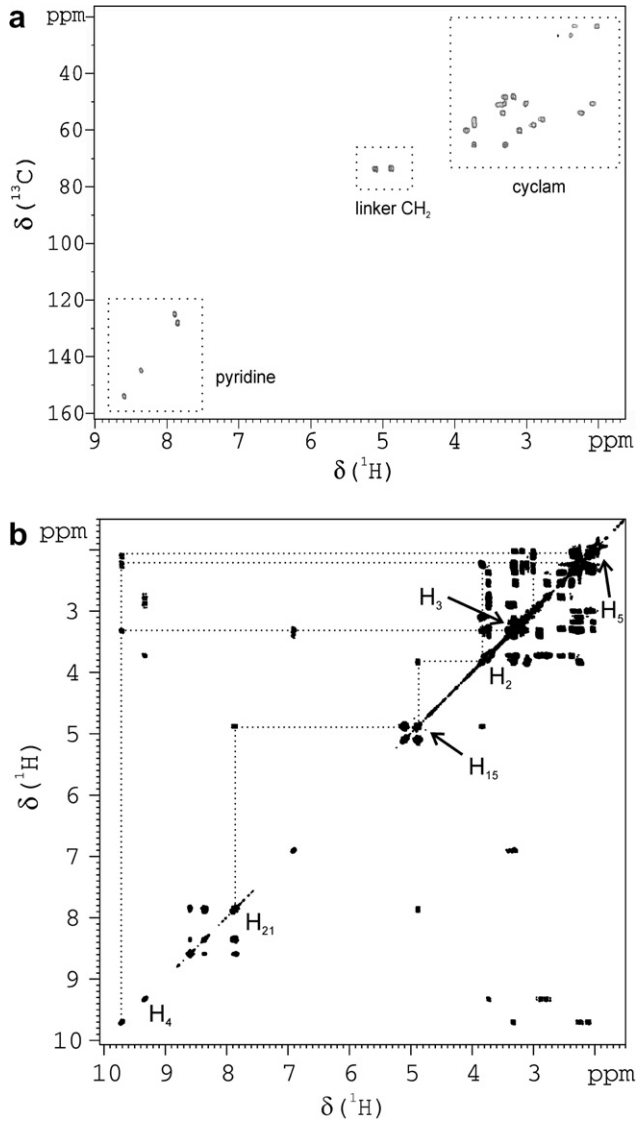

Fig. 2. (a) 2D [^{1}H,^{13}C] HSQC NMR. spectrum of **I** in CD_3CN solution. (b) 2D COSY NMR spectrum of **I** in CD_3CN solution. The dotted lines represent a few steps in the strategy employed in the assignment of the NMR spectrum (see text).

The 2D [^{1}H, ^{13}C] HSQC NMR spectrum (Fig. 2a) shows cross-peaks between 26 of the 29 ^{1}H NMR signals previously described and 16 ^{13}C NMR signals. Among these cross-peaks, it is possible to identify the four single protons from the pyridine moiety, and the 11 paired peaks arising from the geminal CH_2 protons, in agreement with the assignments performed above. Moreover, this NMR experiment confirms the presence of only one spin system (and therefore only one major isomer for **I**) and proved valuable in identifying the geminal pairs of CH_2 protons and assigning them to the corresponding ^{13}C signals.

In combination with all the information gathered up to now, a 2D COSY spectrum (Fig. 2b) allows to find the scalar connectivities and perform a sequential assignment of the ^{1}H NMR spectrum. The pyridine ^{1}H NMR resonance at 7.89 ppm (H_{21}) can be taken as a starting point for the analysis. This proton couples to one that gives rise to a signal at 4.88 ppm, and corresponds to one of the linker methylene protons (H_{15a} or H_{15b}). The latter correlates sequentially with a proton resonating at 3.83 ppm (H_{2a} or H_{2b}). This signal shows additional connectivities with signals at 3.33, 3.09 and 2.23 ppm. From the 2D [^{1}H,^{13}C] HSQC data, protons with chemical shifts of 3.09 and 3.83 ppm are known to be geminal, as well as those at 3.33 and 2.23 ppm. Consequently, these two last resonances can be assigned to their vicinal protons H_{3a}/H_{3b}, both of which are also associated through COSY correlations with the signal at 9.70 ppm. The latter arises from one of the N*H* protons and is now identified as H_4. This proton is scalar-coupled to the one at 2.08 ppm, which in turn couples to a proton at 2.99 ppm. These two last resonances correspond to a pair of geminal protons, that we assign to H_{5a} or H_{5b}. Application of this systematic approach leads to the full assignment of the ^{1}H and ^{13}C NMR spectra. However, the geminal specificity at every CH_2 group still remains unknown. A direct measurement of the $J(^1H^1H)$ coupling constants for these protons helps to eliminate this uncertainty. The *J* values listed in Table 1 reveal two kinds of signals, those split by only one large

Table 1
^{1}H and ^{13}C NMR chemical shifts (δ) in CD_3CN solution, and geminal ^2J(HH) and axial–axial ^3J(HH) scalar coupling constants for compound **I**

^{1}H NMR								^{13}C NMR			
δ (ppm)	Assignment	δ (ppm)	Assignment	δ (ppm)	Assignment	δ (ppm)	Assignment	δ (ppm)	Assignment	δ (ppm)	Assignment
9.70	H_4	4.88	H_{15b}	3.30	H_{7a}	2.37	H_{13b}	161.8	C_{16}	58.2	C_{10}
9.33	H_{11}	3.83	H_{2a}	3.29	H_{14a}	2.33	H_{6a}	153.9	C_{18}	56.2	C_{12}
8.59	H_{18}	3.73	H_{10b}	3.18	H_{7b}	2.23	H_{3a}	144.9	C_{20}	54.0	C_3
8.36	H_{20}	3.71	H_{12b}	3.09	H_{2b}	2.09	H_{5a}	128.1	C_{19}	51.0	C_9
7.89	H_{21}	3.71	H_{14b}	2.99	H_{5b}	2.02	H_{6b}	124.9	C_{21}	50.7	C_5
7.85	H_{19}	3.38	H_{9a}	2.89	H_{10a}			73.6	C_{15}	48.1	C_7
6.91	H_8	3.33	H_{3b}	2.77	H_{12a}			65.2	C_{14}	26.6	C_{13}
5.10	H_{15a}	3.31	H_{9b}	2.54	H_{13a}			60.0	C_2	23.3	C_6

$^2J(H_{15a},H_{15b}) = 17.5$ Hz; $^2J(H_{13a},H_{13b}) = 17.0$ Hz; $^2J(H_{6a},H_{6b}) = 16.4$ Hz; $^2J(H_{7a},H_{7b}) = 15$ Hz; $^2J(H_{2a},H_{2b}) = {}^2J(H_{3a},H_{3b}) = {}^2J(H_{5a},H_{5b}) = 14.0$ Hz; $^2J(H_{9a},H_{9b}) = {}^2J(H_{10a},H_{10b}) = 13.5$ Hz; $^2J(H_{12a},H_{12b}) = {}^2J(H_{14a},H_{14b}) = 13.0$ Hz.

$^3J(H_{2a},H_{3a}) = 14.0$ Hz; $^3J(H_{5a},H_{6a}) = {}^3J(H_{9a},H_{10a}) = 13.5$ Hz; $^3J(H_{6a},H_{7a}) = {}^3J(H_{12a},H_{13a}) = {}^3J(H_{13a},H_{14a}) = 13.0$ Hz; $^3J(H_4,H_{5a}) = {}^3J(H_8,H_{9a}) = {}^3J(H_{10a},H_{11}) = {}^3J(H_{11},H_{12a}) = 11.0$ Hz; $^3J(H_{3a},H_4) = 10.0$ Hz.

^2J(HH) constant, due to geminal coupling exclusively, and those which show at least two large splittings, a ^2J(HH) splitting due to coupling with a geminal partner plus one or two sizeable ^3J(HH) values, depending on whether they are connected to one or two vicinal protons through axial–axial scalar coupling. This information allows discriminating between signals that arise from protons bound to the same carbon atom in the aliphatic backbone. The specific assignment of the methylene N–CH_2-Py resonances requires the study of their dipolar connectivities (see later). Table 1 shows the resulting ^{1}H and ^{13}C NMR assignments.

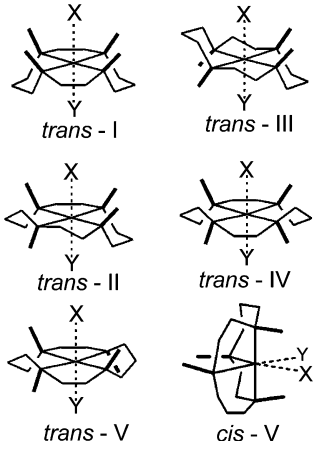

Fig. 3. Different configurations of metal cyclam complexes showing the different alignment of the NH protons.

The NMR analysis presented so far evidences the existence of a single isomer. When attached to a metal center, the macrocyclic 1,4,8,11-tetraazacyclotetradecane (cyclam) could present as much as five configurations at the nitrogen stereogenic centers that give rise to several isomers (labeled *trans*-I–V and *cis*-V, Fig. 3) [29]. In order to determine which of these forms is adopted by compound **I**, a 2D [^{1}H,^{1}H] NOESY NMR data set was recorded in CD_3CN solution. Provided that the difference between configurations resides on the spatial alignment of the NH bonds, special attention has to be paid to these protons. Fig. 4a shows the portion of the NOESY spectrum corresponding to the NH resonances. An intense NOESY cross peak from resonance at 9.70 ppm (H_4) to a signal at 9.33 ppm (H_{11}) indicates that these protons are close in space. They are attached to non-adjacent N atoms and point in the same direction. This observation discards the *trans*-III and *trans*-IV configurations. The remaining NH at 6.91 ppm (H_8) is not dipolar coupled to the other two amine protons (H_{11} or H_4) and is most likely pointing to the opposite side. This last consideration suggests that configurations *trans*-I and *trans*-II should also be disregarded, leaving only two possible configuration, that is *trans*-V or its folded form *cis*-V. The occurrence of NOESY cross-peaks (see Fig. 4b) between protons H_{11}–H_{2a}, H_4–H_{9a}, and H_4–H_{11}

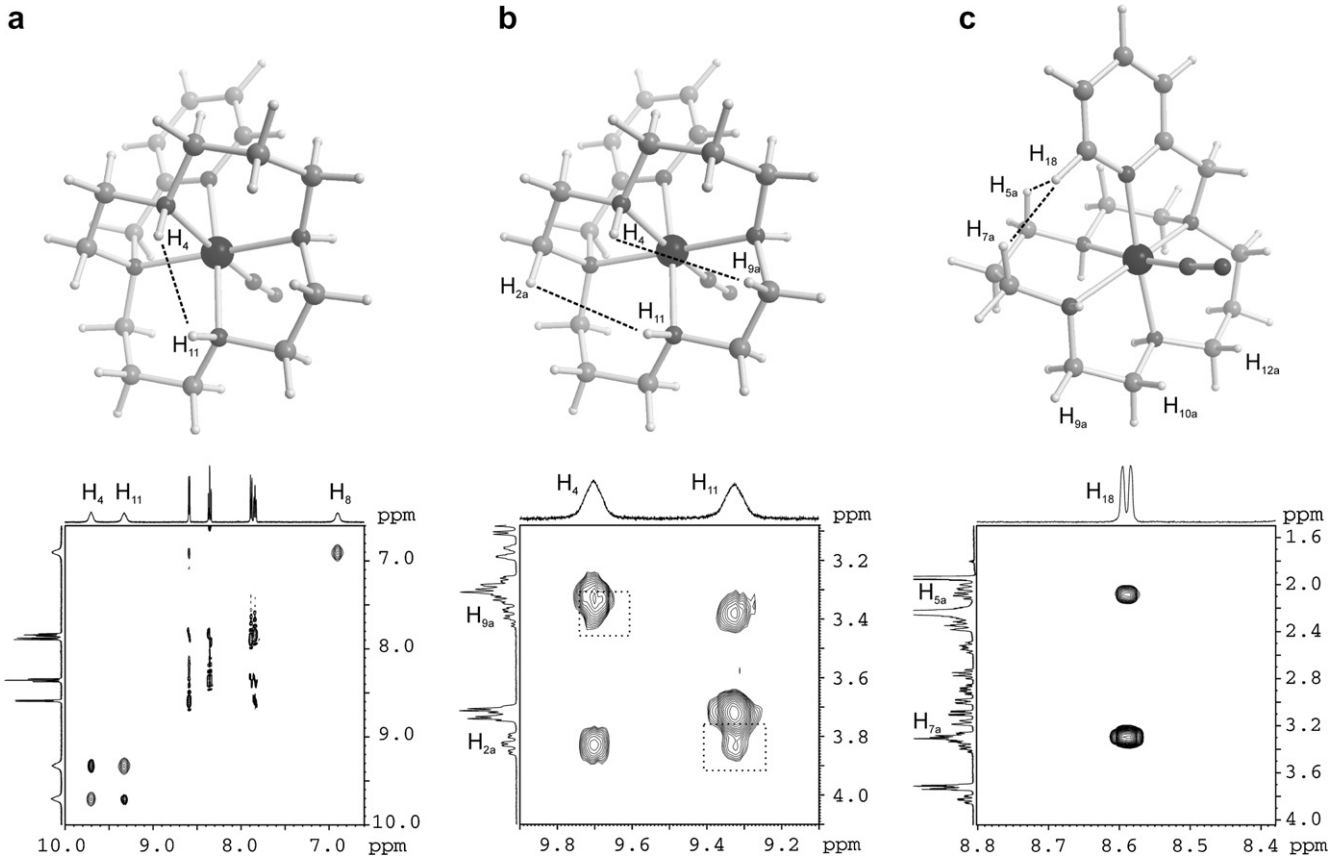

Fig. 4. Selected regions of the 2D [^{1}H,^{1}H] NOESY NMR spectrum of **I** in CD_3CN solution.

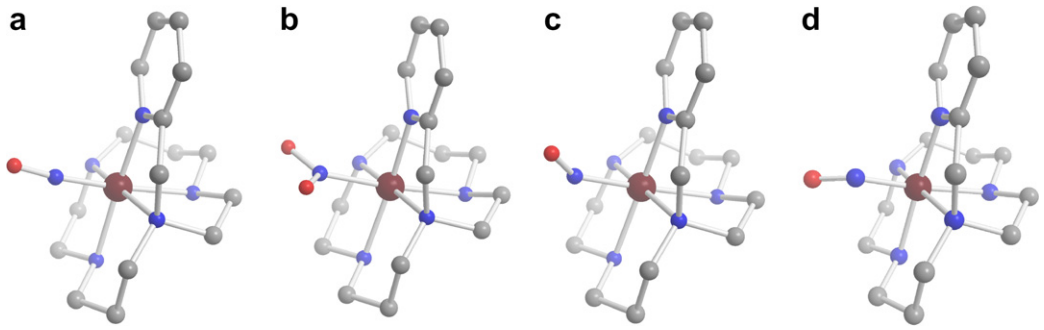

Fig. 5. DFT optimized geometries (in vacuo) for the (a) *cis*-$[Ru(L^{py})NO]^{3+}$ (**I**), (b) *cis*-$[Ru(L^{py})NO_2]^{+}$ (**II**), (c) *cis*-$[Ru(L^{py})NO]^{2+}$ (configuration $\mathbf{III}_a$) and (d) *cis*-$[Ru(L^{py})NO]^{2+}$ (configuration $\mathbf{III}_b$).

disfavors the *trans*-V form. Additionally, the observation of dipolar connectivities between the pyridine H_{18} proton (8.59 ppm) and protons H_{5a} (2.09 ppm) and H_{7a} (3.30 ppm) but not with protons H_{9b}, H_{10a} or H_{12a} (Fig. 4c) confirms a folded *cis*-V configuration. This leaves only two possibilities (actually two pairs of enantiomers) for the structure of **I**, but the only one consistent with all the NMR information and its DFT optimized structure is presented in Fig. 5a. As for the assignment of the methylene N–CH_2-Py protons, the occurrence of NOESY cross-peaks between signals at 4.88 and 3.29 ppm (H_{14a}), and 5.10 and 3.08 ppm (H_{2b}) permitted to know the spatial orientation of these protons. (see Supplementary material for a complete description of the ^{1}H NMR assignment of complex **I**).

It is not trivial to rationalize which factors lead to the isolation of only one configuration. A DFT geometry optimization *in vacuo* of the compound $[Ru(L^{py})Cl]^{+}$ (a presumed intermediate in the preparation of **I**) reveals that the energy of the *cis*-V conformer is *ca.* 10 kJ mol^{-1} lower than the one of the *trans*-III isomer. The situation remains essentially the same if solvation effects are introduced by means of the PCM approximation, where the solvent is treated as a continuum dielectric medium. The computed energy difference suggests a certain degree of thermodynamic control for the reaction. Nevertheless, kinetic effects and even solubility properties cannot be ruled out.

The theoretically optimized *cis*-V geometry obtained for **I**, either in vacuo or with the molecule immersed in a dielectric medium to take into account the influence of the solvent, is consistent with the NMR results. The calculations position the diagnostic H_4–H_{11}, H_4–H_{9a}, H_{11}–H_{2a}, H_{18}–H_{5a}, H_{18}–H_{7a} and H_{18}–H_{9b} pairs of protons at distances of 2.28, 3.06, 3.05, 2.69 and 1.99 Å, respectively. These values are consistent with the observation of the NOESY crossed peaks described above. At the same time, the much larger computed distances H_{18}–H_{9b}, H_{18}–H_{10a} and H_{18}–H_{12b} of 5.05, 5.42 and 6.24 Å, respectively, explain the lack of signals for these proton pairs. Table 2 contains some relevant computed structural parameters and Fig. 5a displays the geometry of the optimized cation. The ruthenium atom is placed in a distorted octahedral N_6 environment, generated by the nitrosyl ligand and the five donor nitrogen atoms of the substituted macrocycle. The Ru–N(nitrosyl) (labeled Ru–N_{22}) bond reveals as significantly shorter than the five remaining Ru–N bonds. The Mayer bond order [30] for this bond (1.08) confirms the higher degree of covalency for Ru–N_{22} compared to the Ru–N(amine) (average of 0.52) and Ru–N(py) (0.53) bonds in the same compound. The computed N_{22}–O_{23} distance and the linear nature of the RuNO moiety are consistent with the expectations for a $\{RuNO\}^6$ species [3,31].

3.2. Vibrational and electronic spectroscopy

The IR spectrum of $[Ru(L^{py})NO](PF_6)_3$ in a KBr disk displays a sharp intense band at 1917 cm^{-1}, assignable to the N–O stretching vibration, ν_{NO}. This value is slightly higher than the ones found for *trans*-[Ru(NO)Cl(cyclam)]$(PF_6)_2$ (1875 cm^{-1}) [32] and $[Ru^{II}(NH_3)_5(NO)]Br_3$ (1913 cm^{-1}) [33], comparable to those reported for several *cis*- and *trans*-$[Ru(NH_3)_4L(NO)]^{3+}$ species (1923–1942 cm^{-1}) [6], and smaller than the values observed in other Ru(II) compounds that carry electron-withdrawing co-ligands (1946 and 1959 cm^{-1} for [Ru(trpy)(bpy)(NO)]-$(PF_6)_3$ and [Ru(tpm)(bpy)(NO)]$(ClO_4)_3$, respectively) [9,11]. This ν_{NO} frequency has been usually employed to qualitatively establish the degree of electronic interaction between the NO ligand and the metal center. In this case the ν_{NO} value suggests an $[Ru^{II}NO^{+}]$ electronic distribution where the NO^{+} character is well preserved [2], in agreement with the DFT bonding picture. The calculated frequency of 1849 cm^{-1} is lower than the measured one. Though this discrepancy is not unusual for calculations at this level of theory [10,11,13,14,24], there might be some contribution to the observed difference arising from hydrogen-bond interactions in the solid state.

The spectral region between 750 and 900 cm^{-1} has been usually employed to differentiate between *cis* and *trans* geometries in cyclam compounds [34,35]. In our case, besides this region is partially obscured by the PF_6^- vibrations, the pendant-arm leaves the complex with no symmetry elements no matter the configuration of the macrocycle. For this reason, the number of signals does not depend on the cyclam configuration and the low energy N–H vibrations are not informative.

Table 2
Selected bond lengths and angles for **I**, **II** and **III** obtained from the DFT optimized structures

Distance	I in vacuo (Å)	I in H_2O (Å)	I in acn (Å)	II in vacuo (Å)	III_a in vacuo (Å)	III_b in vacuo (Å)
$Ru–N_1$	2.17	2.17	2.17	2.19	2.17	2.17
$Ru–N_4$	2.17	2.16	2.16	2.20	2.21	2.21
$Ru–N_8$	2.23	2.20	2.20	2.19	2.22	2.21
$Ru–N_{11}$	2.17	2.15	2.15	2.18	2.17	2.17
$Ru–N_{17}$	2.15	2.15	2.14	2.13	2.14	2.15
$Ru–N_{22}$	1.79	1.78	1.78	2.04	1.90	1.90
$N_{22}–O_{23}$	1.18	1.18	1.18	1.29	1.22	1.22
$N_{22}–O_{24}$				1.31		
Angle	**I in vacuo (°)**	**I in H_2O (°)**	**I in acn (°)**	**II in vacuo (°)**	**III_a in vacuo (°)**	**III_b in vacuo (°)**
$Ru–N_{22}–O_{23}$	174.3	174.7	174.4	122.7	141.6	144.7
$Ru–N_{22}–O_{24}$				118.3		
$O_{23}–N_{22}–O_{24}$				118.8		
$N_1–Ru–N_8$	168.9	170.1	170.0	173.9	171.9	171.6
$N_4–Ru–N_{22}$	174.9	175.7	175.5	175.5	176.5	176.0
$N_{11}–Ru–N_{17}$	174.6	174.6	174.4	172.8	174.3	174.4
$N_1–Ru–N_4$	82.3	82.3	82.3	83.2	82.8	82.8
$N_1–Ru–N_{11}$	93.7	93.8	93.4	95.2	95.1	94.6
$N_1–Ru–N_{17}$	80.9	80.8	81.0	80.9	80.7	80.6
$N_1–Ru–N_{22}$	96.4	96.6	96.5	97.5	95.1	95.4
$N_4–Ru–N_8$	88.1	89.0	88.9	92.3	90.4	90.3
$N_4–Ru–N_{11}$	92.8	91.4	91.4	94.8	94.0	93.5
$N_4–Ru–N_{17}$	86.9	87.2	87.0	90.7	89.4	88.8
$N_8–Ru–N_{11}$	81.0	81.7	82.0	81.1	81.0	80.9
$N_8–Ru–N_{17}$	104.4	103.5	103.4	103.3	103.6	104.2
$N_8–Ru–N_{22}$	93.6	92.4	92.7	87.3	91.9	91.8
$N_{11}–Ru–N_{22}$	92.3	92.9	93.1	89.5	89.0	90.1
$N_{17}–Ru–N_{22}$	88.0	88.5	88.5	85.1	87.5	87.5
$N_{17}–Ru–N_{22}–O_{23}$	−10.4	−16.4	−9.9	86.8	25.2	−147.4
$C_{18}–N_{17}–Ru–N_8$	−2.7	−1.0	−2.0	1.1	0.7	0.7
$C_{16}–N_{17}–Ru–N_8$	−179.4	−178.5	179.7	−174.0	−176.2	−175.5

Fig. 6 displays the electronic spectra of **I** in water (pH 1.0, $HClO_4$) and acetonitrile. Apart from the complete lack of strong bands in the visible region of the spectrum, the most remarkable features when the spectrum was recorded in water include intense absorptions in the UV region, a slight shoulder at *ca.* 236 nm ($\varepsilon = 5770\ M^{-1}\ cm^{-1}$), a much better resolved transition at *ca.* 257 nm ($\varepsilon = 4660\ M^{-1}\ cm^{-1}$), and a progression of weak bands at 313 nm (sh, $\varepsilon = 335\ M^{-1}\ cm^{-1}$), 355 nm (sh, $\varepsilon = 110\ M^{-1}\ cm^{-1}$) and 450 nm ($\varepsilon = 40\ M^{-1}\ cm^{-1}$). Ru(II) species holding amine ligands usually display solvent dependent electronic spectroscopy due to solute–solvent specific (hydrogen-bonding) interactions that can modulate the electronic density on the metal ion [36–39]. This same effect was described for species containing cyclam and π-acceptor ligands [35,40,41]. However, the spectrum of **I** in acetonitrile is virtually identical to the one measured in water, with only minor shifts of the bands to 232 nm ($\varepsilon = 6475\ M^{-1}\ cm^{-1}$), 258 nm ($\varepsilon = 4900\ M^{-1}\ cm^{-1}$), 317 nm (sh, $\varepsilon = 420\ M^{-1}\ cm^{-1}$), 350 nm (sh, $\varepsilon = 180\ M^{-1}\ cm^{-1}$) and 445 nm ($\varepsilon = 40\ M^{-1}\ cm^{-1}$).

The calculations establish that the HOMO is mainly located on the pyridine ring. The degeneracy of the t_{2g} set of metal orbitals is fully lifted because of the symmetry of the compound. One of these orbitals is not properly oriented and remains essentially non-bonding with respect to the nitrosyl moiety, being the majority component of the HOMO − 1 molecular orbital. The other two are strongly stabilized because of the fairly strong π interactions with the nitrosyl, and appear as the main constituents of the bonding HOMO − 5 and HOMO − 6 molecular orbitals. Conversely the LUMO and LUMO + 1 orbitals are mainly located on the NO fragment, but have some metal character resulting from the interaction between the π^* orbitals of the nitrosyl group with $t_{2g}(d_\pi)$ metal orbitals. Thus, the back-donation to the nitrosyl partially shifts electronic density from the metal ion into the π^* orbitals of the coordinated NO^+. The stabilization of the metal centered orbitals and the destabilization of the nitrosyl ones enlarge the HOMO–LUMO energy difference up to 3.2 and 3.6 eV, estimated in vacuum and in solution, respectively. These large values are responsible for the shift of the electronic spectrum to higher energies. The $Ru(II) \rightarrow \pi_{py}$ transition normally expected in the visible region [36–39] is therefore not observed there, but probably at much higher energy. We were not able to observe this band in our experimental conditions, but the analogous transition has been reported at 230 nm in the related systems $[Ru(NH_3)_4L(NO)]^{3+}$ (L = isonicotinamide or pyrazine) [6a,6b]. The π back-donation effect overcomes the subtle electronic changes expected to be induced by the specific interactions with the solvent. This explains the insensitivity of the electronic spectrum toward solvent changes.

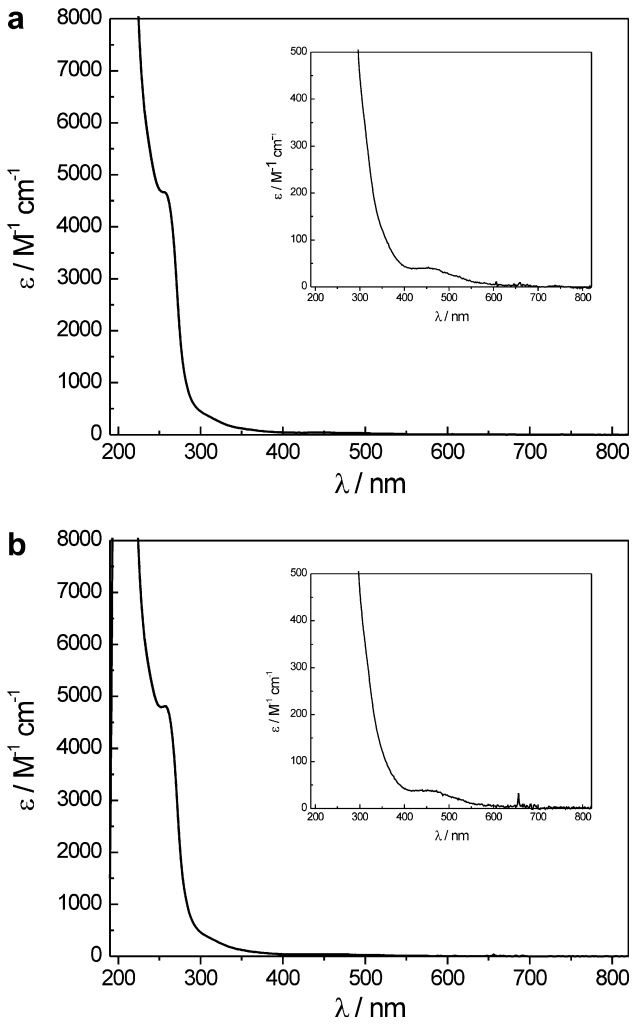

Fig. 6. Experimental UV–Vis spectra of **I** in water and organic medium. (a) Aqueous $HClO_4$ 0.1 M, (b) acetonitrile.

The interpretation of the electronic spectra of nitrosyl complexes is not unambiguous. In our case, the low symmetry of the species might lead to substantial orbital mixing that further complicates the analysis. (TD)DFT has proven as a valuable tool to assist in the assignment of the spectra of several related species [6c]. In the case of **I**, the calculated transitions reproduce qualitatively the experimental spectra. The computations position the Ru(II) $\rightarrow \pi_{py}$ MLCT at 208 nm, though superimposed with d–d and ligand-based transitions, and the lowest lying $\pi_{py} \rightarrow \pi^*_{py}$ intraligand transition at 257 nm. The extra features at lower energy involve several weak transitions with mixed d–d, MLCT (Ru(II) $\rightarrow \pi^*_{NO}$) and LL′CT ($\pi_{py} \rightarrow \pi^*_{NO}$) character. The agreement between the computed and experimental spectra is very good and supports the theoretical treatment.

3.3. Reactions with nucleophiles: formation of $[Ru(L^{py})NO_2]^+$

In spite of the backbonding effect, the coordinated nitrosyl still has a large nitrosonium character. The $[Ru^{II}NO^+]$ electronic distribution manifests experimentally not only in the ν_{NO} values, but also in the expected reaction of **I** with nucleophiles [5,26]. Aqueous solutions of **I** in non-acidic medium undergo rapid spectral changes with formation of $[Ru(L^{py})NO_2]^+$ (**II**), as described by Eq. (1). The reaction with OH^- is reversible and a full recovery of the nitrosyl reactant can be achieved upon acidification. Fig. 7 displays the spectra recorded in the stepwise conversion of the nitrosyl into the nitro compound. The presence of well defined isosbestic points suggests the absence of processes other than the one of interest. A multi-wavelength treatment of the absorption spectra by factor analysis also reveals the presence of only two colored species. This kind of reactions has been extensively studied in the past [5,26–28]. The nucleophilic attack of an OH^- ion leads to the formation of a covalent N–O bond. Afterwards, the intermediate nitrous acid complex deprotonates to yield the nitro derivative [9–11,28,42].

The spectrum of **II** is dominated by strong absorption bands at 264 nm ($\varepsilon = 4260\ M^{-1}\ cm^{-1}$), 308 nm ($\varepsilon = 4440\ M^{-1}\ cm^{-1}$) and 474 nm ($\varepsilon = 5590\ M^{-1}\ cm^{-1}$). As a comparison, the related compound *trans*-$[Ru(NH_3)_4(4\text{-Mepy})(NO_2)]^+$ (4-Mepy = 4-methyl pyridine) displays only one broad MLCT band at 378 nm with a shoulder at higher energies [10].

To understand the electronic structure of this species, we performed a theoretical geometry optimization, whose results are summarized in Table 2 and Fig. 5b. The coordination sphere of the Ru(II) ion in **II** remains very similar to the one described for **I**. The stable structure shows a dihedral N(py)–Ru–N–O angle close to 90° and a slight asymmetry in the coordinated NO_2^-, probably due to the intramolecular hydrogen-bond interaction with the closest N–H at *ca.* 2 Å. A full scan of this dihedral angle shows two minima in the potential energy surface. They correspond to equivalent geometries that result from a 180°

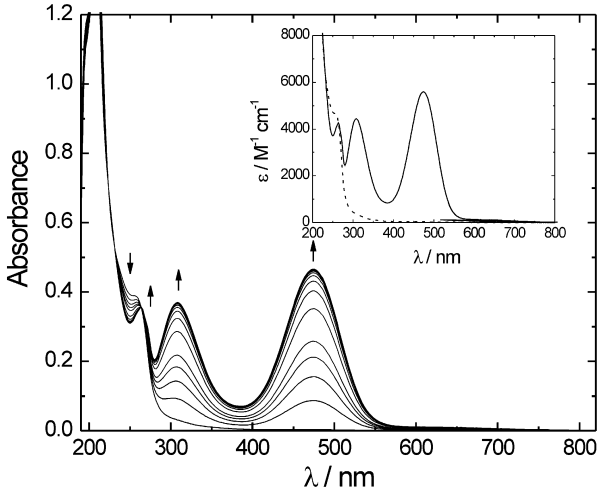

Fig. 7. Consecutive spectra for the reaction of **I** with OH^-. $[OH^-] = ca.\ 10^{-6}$ M, [complex] $= 8.4 \times 10^{-5}$ M. The arrows indicate the spectral changes along the reaction. Inset: Deconvoluted spectra of **I** (dashed line) and **III** (full line).

rotation of the NO_2^- moiety around the Ru–N axis followed by relaxation of the internal coordinates. These two minima are separated by a barrier of 33 kJ mol^{-1} (in vacuo), suggesting that the coordinated nitrite is not freely rotating in this species (or at least rotation around this axis has to be very slow in solution).

The nitro group is a poorer π-acceptor than the nitrosyl (and a better σ-donor). This results in an overall electronic picture with a lower degree of metal–ligand covalency and a higher electronic density located on the metal, as revealed by an average Mayer bond order of 0.36 for Ru–N(cyclam) and 0.49 for $Ru–N_{22}$. The filled frontier orbitals can now be clearly identified as the t_{2g} set. The lowest lying empty molecular orbitals are mostly located on the pyridine and the NO_2^- fragments, but to our surprise the calculations revealed a substantial degree of mixing between pyridine- and nitro-centered orbitals, feasible because of the low symmetry of this species.

The (TD)DFT calculated energy and intensity of the MLCT transitions does not accurately reproduce the experimental observations. This is not completely unexpected, because the electronic structure of this species has to be more sensitive to the medium. Consequently, the theoretical prediction of the electronic spectrum becomes much more difficult. Several approaches [38,43] have been employed in the past to deal with solute–solvent specific interactions, but the implementation of these strategies is beyond the scope of this manuscript. We perform here a tentative assignment of the donor–acceptor charge transfer spectroscopy employing qualitative arguments and comparing with related systems.

The literature values for the MLCT maxima of $[Ru(NH_3)_5NO_2]^+$ and $[Ru(NH_3)_5py]^{2+}$ in water are 368 and 407 nm, respectively [44]. The substitution of an ammonia by the poorer σ-donor pyridine molecule in the coordination sphere of $[Ru(NH_3)_5NO_2]^+$ is expected to shift the $Ru(II) \rightarrow NO_2^-$ MLCT band to higher energies. Using the same argument, the replacement of an ammonia by a nitrite should shift also the band to higher energies (lower wavelengths) than in $[Ru(NH_3)_5py]^{2+}$. This explains reasonably the occurrence of only one band in the spectrum of *trans*-$[Ru(NH_3)_4(4\text{-Mepy})(NO_2)]^+$ that results from the overlap of a $Ru(II) \rightarrow \pi_{py}$ and a $Ru(II) \rightarrow NO_2^-$ absorption both shifted to higher energy if compared to the pentaamine case.

The substantial mixing between the acceptor fragments suggested by the DFT calculations perturbs this description, shifting the two CT bands in opposite directions. We therefore assign the 308 nm band as involving the coordinated nitrite as the acceptor fragment and the 474 nm one as arising from a $Ru(II) \rightarrow \pi_{py}$ MLCT, both of them shifted with respect of the ones in *trans*-$[Ru(NH_3)_4(4\text{-Mepy})(NO_2)]^+$ as a consequence of the orbital mixing.

3.4. $\{RuNO\}^{6,7}$ interconversion

The cyclic voltammogram of **I** in aqueous solution (pH 1, $HClO_4$, $\mu = 0.1$ M) shown in Fig. 8a displays a single reversible wave at −0.02 V, arising from the one-electron interconversion between **I** and the $\{RuNO\}^7$ species $[Ru(L^{py})NO]^{2+}$ (**III**). Further exploration at more reducing potentials was not attempted because of the solvent electrochemical window.

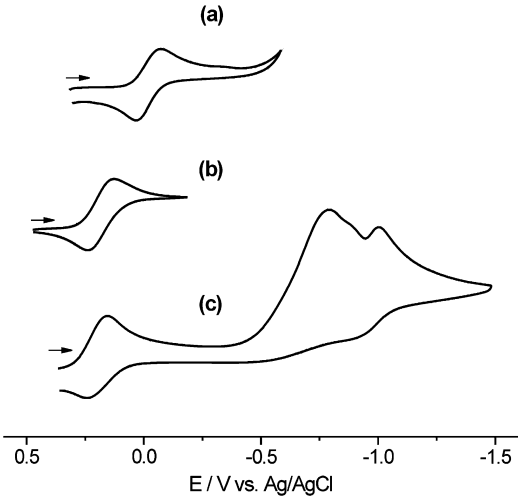

Fig. 8. Cyclic voltammograms of I in H_2O/0.1 M $HClO_4$ (a) and acetonitrile/0.1 M $TBAPF_6$ solution (b and c). Conditions: glassy carbon working electrode, scan rate 200 mV s^{-1}. The arrows indicate the direction of the scan.

The observed redox potential for the reduction of the coordinated nitrosyl is higher than the one reported for the related *trans*-$[Ru(NH_3)_4(4\text{-Mepy})(NO)]^{3+}$, −0.25 V ($\mu = 0.1$ M CF_3COOH/CF_3COONa, pH 4). Even when the difference might be partially ascribed to the differences between *cis*- and *trans*-configurations, it should be noted that a similar shift, which might originate in solvation issues related to the macrocylic ligand was reported when comparing other tetrammine- and cyclam-based nitrosyls [32,35]. For these related systems, the cyclic voltammograms reveal a series of chemical reactions coupled to the electron transfer process, that have been interpreted in terms of labilization of the co-ligands and NO^0 [6,32,35,45]. None of these complications seems to be associated to the $\{RuNO\}^{6,7}$ conversion in our system.

The cyclic voltammograms in acetonitrile (Fig. 9b) reveal the same reversible one-electron reversible process, though shifted to $E^0 = 0.18$ V. An increase of 0.125 V was reported for the same process in *trans*-[Ru(NO)Cl(cyclam)]$^{2+}$, and an even larger difference of *ca.* 0.30 V has been measured in $[Ru(tpm)(bpy)NO]^{3+}$ [11]. The differences can be traced back to changes in the dielectric properties of the solvents, which would favor the reduction process in less polar media. In addition, the larger donor number (DN)[46] of water if compared to acetonitrile (18.1 versus 14.1 for water and acetonitrile, respectively) contributes to increase the electronic density in the coordinated nitrosyl, via specific hydrogen-bond interaction with the amine protons [36]. The general increment in the redox potential, combined with a wider electrochemical window than in water, allowed to explore the reduction of the

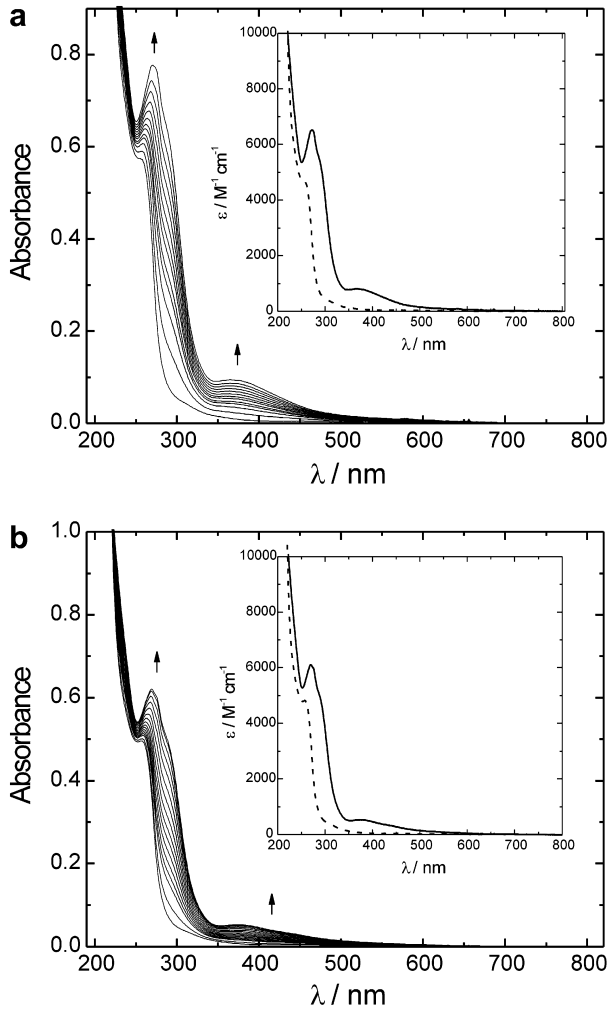

Fig. 9. Spectroelectrochemical conversion of **I** into **III** in water and organic medium under controlled potential conditions. (a) Aqueous $HClO_4$ 0.1 M, (b) acetonitrile/0.1 M $TBAPF_6$, [complex] = 1.2×10^{-4} M and 1.0×10^{-4} M for water and acetonitrile, respectively. The arrows indicate the spectral changes upon reduction. Insets: deconvoluted spectra for **I** (dashed line) and **III** (full line) obtained by factor analysis (see text).

$\{RuNO\}^7$ species. At more negative potentials (*ca.* −0.75 V) a complex pattern involving consecutive electron transfer processes can be detected. All this extra waves appear as irreversible in the CV time scale. The first of such electron transfer process might be tentatively ascribed to the formation of a $\{RuNO\}^8$ species [8,14]. This species appears to be unstable in the CV timescale, even if the experiments are performed at −30 °C and some complementary characterization would be required in order to improve its description.

Fig. 9 shows the stepwise **I** → **III** conversion under controlled potential conditions both in acidic conditions and in acetonitrile solution. The reduction processes proceed smoothly, and the factor analysis of the recorded spectra reveals only two colored species in both solvents. The integrated current, as well as the absorbance versus open-circuit potential curves obtained during the electrolysis are also consistent with a 1-electron process with $E^0_{NO+/NO} = -0.02$ and 0.21 V for water and acetonitrile, respectively. These values are in very good agreement with the ones obtained in the cyclic voltammetry experiments. The slight shift detected in acetonitrile is mostly due to the different temperatures employed in both determination. This experiment confirms the reversibility of the $\{RuNO\}^{6,7}$ redox interconversion. The electrogenerated reduced species in aqueous solution seems to be stable if protected from oxygen, but reoxidizes rapidly in the presence of air to quantitatively regenerate **I**. In acetonitrile, the oxidation by molecular oxygen is much slower, and no spectral changes were observed in the minute timescale. Electrochemical reoxidation leads, in both cases, to quantitative recovery of **I,** even after 2 h. The reversibility of the NO^+/NO conversion indicates that the whole coordination sphere in **III** (including the coordinated NO·) is strongly inert toward substitution reactions. As we mentioned above, this is not always the case, and release of NO or NO-induced *trans* labilization has been observed for several complexes [32,35]. The spectroelectrochemistry confirms that this is not the case with **III**, making this system particularly useful to be studied in both $\{RuNO\}^{6,7}$ oxidation states.

One-electron reduction is expected to induce a bending of the Ru–N–O angle [2,3]. A DFT geometry optimization confirms this expectation. The computation performed in vacuo included a potential energy surface scan of the dihedral O–N–Ru–N(py) angle, which revealed two possible stable geometries $\mathbf{III}_a$ and $\mathbf{III}_b$ for this $\{RuNO\}^7$ species (Fig. 5). The two situations minimize the steric interactions between the NO fragment and the L^{py} ligand. In contrast with **II** and other $\{MNO\}^7$ systems [14], there seem to be no signs of intramolecular N–O ⋯ H–N(cyclam) hydrogen-bond. These two conformers have slightly different thermodynamic stabilities, with $\mathbf{III}_a$ laying 5.4 kJ mol^{-1} below $\mathbf{III}_b$. Overall, the potential energy surface is rather flat and the interconversion of $\mathbf{III}_a$ into $\mathbf{III}_b$ involves a small energy barrier of 6.7 kJ mol^{-1} (1.3 kJ mol^{-1} in the opposite direction). Even when the presence of solvent molecules interacting specifically with the amine protons might hinder the interconversion between conformers, our calculations imply that the NO fragment is freely rotating in the $\{RuNO\}^7$ species. Table 2. collects the most significant structural parameters for $\mathbf{III}_a$ and $\mathbf{III}_b$. The overall features are very similar for both, with a practically identical co-ligand environment. The most significant structural change upon reduction involve, as expected, the lengthening of the Ru–N_{22} and N_{22}–O_{23} to 1.90 and 1.22 Å, and the bending of the Ru–N_{22}–O_{23} angle to *ca.* 143°. These parameters, combined with the reduction of the N_{22}–O_{23} Mayer bond order to 1.56 reflect the population of a formally π-antibonding orbital located mostly on the NO fragment. In fact, the calculations confirm that the SOMO is mostly located on the NO fragment with partial delocalization onto the metal center, a common feature to many $\{RuNO\}^7$ species [9,11,12,16].

The calculations also reveal an overall reduction of the covalency of the Ru–N(L^{py}) bonds, which show an average Mayer bond order of 0.41. Particularly, the Ru–N_4 bond order of 0.38 is the lowest, suggesting the onset of a *trans*-effect. In spite of this, the coordination sphere remains structurally unaffected due to the rigidity of the whole macrocyle. The electronic structure of this species is also affected by π-backbonding. Two metallic orbitals belonging to the t_{2g} set reveal some degree of mixing with the π^* orbitals located on the NO fragment, while the third remains as non-bonding because of the symmetry of the complex. The backbonding interaction is overall smaller than in **I**, revealing NO as a poorer π-acceptor. The lowest lying empty molecular orbitals correspond essentially to the ligand-centered π^* orbitals. Their relatively low energy, in contrast with the computations performed on **I**, permit the development of CT transitions in the visible region. The electronic spectrum of **III** displays an intense absorption at 271 nm ($\varepsilon = 6500\ M^{-1}\ cm^{-1}$), a shoulder at 287 nm ($\varepsilon = 5500\ M^{-1}\ cm^{-1}$) and a weaker band at 365 nm ($\varepsilon = 810\ M^{-1}\ cm^{-1}$), when recorded in water. In acetonitrile the positions of these bands remain almost unchanged at 270 nm ($\varepsilon = 6100\ M^{-1}\ cm^{-1}$), 287 nm ($\varepsilon = 5010\ M^{-1}\ cm^{-1}$) and 369 nm ($\varepsilon = 520\ M^{-1}\ cm^{-1}$).

The (TD)DFT results suggest that the low energy bands, predicted at 378 nm and observed at *ca.* 365 nm are better described as the spin-allowed $\pi_{NO} \rightarrow d_{Ru}$ LMCT with some $\pi_{NO} \rightarrow \pi^*_{py}$ character. The same computations assign the intense absorption at *ca.* 270–290 nm as arising from a $d_{Ru} \rightarrow \pi^*_{py}$ transition, though extensively overlapped with the intraligand $\pi_{py} \rightarrow \pi^*_{py}$, the $d_{Ru} \rightarrow \pi^*_{NO}$ MLCT and weak d–d transitions. It is surprising that even when the absorption bans appear to have CT character, there seems to be little solvent dependency. Though this fact can be indicative of extensive π-backbonding interactions [36,38,39,47], it is not clear that this is the case for **III** and a broader range of solvents has to be explored to asses this issue.

4. Conclusions

This pendant-arm cyclam complex of Ru(II) proved as a valuable platform to investigate the NO^+/NO^0 redox chemistry. The marked inertness of the coordination sphere on both $\{RuNO\}^6$ and $\{RuNO\}^7$ oxidation states, the strong color changes associated to the redox processes and the preliminary results concerning the reaction of this species with O_2 are promising, and open the possibility to a systematic study of redox reactivity. Variations in the identity of the pendant-arm could be used in the future to generate a series of nitrosyl compounds with control over $E^0_{NO^+/NO^0}$ in a region of potentials with scarce examples in the literature.

The abundant experience in connection with the derivatization of cyclam envisages many possible variations leading to macrocyclic species with different donor/acceptor capabilities. The parallelism with the related *trans*-$[Ru(NH_3)_4(4\text{-Mepy})(NO)]^{3+}$ and *trans*-$[Ru(NO)Cl(cyclam)]^{2+}$ series of compounds and the use of theoretical approaches as the ones employed here stand as valuable predictive tools that might be of significant help in the selection of the appropriate substituents. We are currently exploring this possibility.

Acknowledgements

The authors thank the University of Buenos Aires (UBA), the Consejo Nacional de Investigaciones Científicas y Técnicas (CONICET), the Agencia Nacional de Promoción Científica y Tecnológica (ANPCyT) and Fundación Antorchas for economic funding. LDS is a member of the scientific staff of CONICET and AGD is a graduate fellow from UBA.

Appendix A. Supplementary material

IR spectrum of *cis*-$[Ru(L^{py})NO](PF_6)_3$ in the solid state (KBr pellet), ^1H NMR and ^{13}C NMR spectra in CD3CN and full proton assignments. Supplementary data associated with this article can be found, in the online version, at doi:10.1016/j.poly.2007.04.038.

References

[1] G.B. Richter-Addo, P. Legzdins, Metal Nitrosyls, Oxford University Press, New York, 1992.
[2] J.A. Olabe, L.D. Slep, in: J.A. Mc Cleverty, T.J. Meyer (Eds.), Comprehensive Coordination Chemistry II, from Biology to Nanotechnology, vol. 1, Elsevier, Oxford, 2004, p. 603.
[3] (a) J.H. Enemark, R.D. Feltham, Coord. Chem. Rev. 13 (1974) 339;
(b) J.H. Enemark, R.D. Feltham, Top. Stereochem. 12 (1981) 155.
[4] (a) N.J. Armor, M.Z. Hoffman, Inorg. Chem. 14 (1975) 444;
(b) H. Nagao, H. Nishimura, H. Funato, Y. Ichikawa, F.S. Howell, M. Mukaida, H. Kakihana, Inorg. Chem. 28 (1989) 3955;
(c) H. Nishimura, H. Matsuzawa, T. Togano, M. Mukaida, H. Kakihana, F. Bottomley, J. Chem. Soc., Dalton Trans. (1990) 137.
[5] F. Bottomley, Acc. Chem. Res. 11 (1978) 158.
[6] (a) M.G. Gomes, C.U. Davanzo, S.C. Silva, L.G.F. Lopez, P.S. Santos, D.W. Franco, J. Chem. Soc., Dalton Trans. (1998) 601;
(b) S.D.S. Borges, C.U. Davanzo, E.E. Castellano, J. Z-Schpector, S.C. Silva, D.W. Franco, Inorg. Chem. 37 (1998) 2670;
(c) S.I. Gorelsky, S.C. DaSilva, A.B.P. Lever, D.W. Franco, Inorg. Chim. Acta 300–302 (2000) 698.
[7] (a) F. Baumann, W. Kaim, L.M. Baraldo, L.D. Slep, J.A. Olabe, J. Fiedler, Inorg. Chim. Acta 285 (1999) 129;
(b) M. Wanner, T. Scheiring, W. Kaim, L.D. Slep, L.M. Baraldo, J.A. Olabe, S. Zalis, E.J. Baerends, Inorg. Chem. 40 (2001) 5704.
[8] C. Hauser, T. Glaser, E. Bill, T. Weyhermuller, K. Wieghardt, J. Am. Chem. Soc. 122 (2000) 4352.
[9] F. Roncaroli, L.M. Baraldo, L.D. Slep, J.A. Olabe, Inorg. Chem. 41 (2002) 1930.
[10] F. Roncaroli, M.E. Ruggiero, D.W. Franco, G.L. Estiu, J.A. Olabe, Inorg. Chem. 41 (2002) 5760.
[11] M. Videla, J.S. Jacinto, R. Baggio, M.T. Garland, P. Singh, W. Kaim, L.D. Slep, J.A. Olabe, Inorg. Chem. 45 (2006) 8608.
[12] B.R. McGarvey, A.A. Ferro, E. Tfouni, C.W.B. Bezerra, I. Bagatin, D.W. Franco, Inorg. Chem. 39 (2000) 3577.

[13] M. Li, D. Bonnet, E. Bill, F. Neese, T. Weyhermuller, N. Blum, D. Sellman, K. Wieghardt, Inorg. Chem. 41 (2002) 3444.
[14] R.G. Serres, C.A. Grapperhaus, E. Bothe, E. Bill, T. Weyhermuller, F. Neese, K. Wieghardt, J. Am. Chem. Soc. 126 (2004) 5138.
[15] M. Videla, F. Roncaroli, L.D. Slep, J.A. Olabe, J. Am. Chem. Soc. 129 (2007) 278.
[16] S. Frantz, B. Sarkar, M. Sieger, W. Kaim, F. Roncaroli, J.A. Olabe, S. Zalis, Eur. J. Inorg. Chem. (2004) 2902.
[17] I.P. Evans, A. Spencer, G. Wilkinson, J. Chem. Soc., Dalton Trans. (1973) 204.
[18] I. Meunier, A.K. Mishra, B. Hanquet, P. Cocolios, R. Guilard, Can. J. Chem., Rev. Can. Chim. 73 (1995) 685.
[19] A.J. Bard, L.R. Faulkner, Electrochemical Methods, Fundamentals and Applications, John Wiley & Sons, Inc., New York, 1980.
[20] I. Noviandri, K.N. Brown, D.S. Fleming, P.T. Gulyas, P.A. Lay, A.F. Masters, L. Phillips, J. Phys. Chem. B 103 (1999) 6713.
[21] E.R. Malinovsky, Factor Analysis in Chemistry, 2nd edn., Wiley-Interscience, New York, 1991.
[22] A.R. Parise, S. Pollak, L.D. Slep, J.A. Olabe, An. Asoc. Quim. Argent. 83 (1995) 211.
[23] M.J. Frisch et al., Gaussian 03, Rev. D01, Gaussian, Inc., Wallingford CT, 2004.
[24] J. Li, L. Noodleman, D.A. Case, in: E.I. Solomon, A.B.P. Lever (Eds.), Inorganic Electronic Structure and Spectroscopy, vol. I, John Wiley & Sons, New York, 1999, p. 661.
[25] N.F. Curtis, in: J.A. Mc Cleverty, T.J. Meyer (Eds.), Comprehensive Coordination Chemistry II, from Biology to Nanotechnology, vol. 1, Elsevier, Oxford, 2004, p. 447.
[26] F. Bottomley, in: P.S. Braterman (Ed.), Reactions of Coordinated Ligands, vol. 2, Plenum Publ. Corp., New york, 1989.
[27] (a) F. Bottomley, M. Mukaida, J. Chem. Soc., Dalton Trans. (1982) 1933;
(b) P.C. Ford, I.M. Lorkovic, Chem. Rev. 102 (2002) 993;
(c) P.C. Ford, L. Laverman, I. Lorkovic, Adv. Inorg. Chem. 54 (2003) 203;
(d) M.D. Lim, I. Lorkovic, P.C. Ford, J. Inorg. Biochem. 99 (2005) 151.
[28] A.A. Chevalier, L.A. Gentil, J.A. Olabe, J. Chem. Soc., Dalton Trans. (1991) 1959.
[29] B. Bosnich, C.K. Poon, M.L. Tobe, Inorg. Chem. 4 (1965) 1102.
[30] A. Szabo, N.S. Ostlund, Modern Quantum Chemistry. Introduction Advanced Electronic Structure Theory, 1st edn., Dover Publications, Inc., Mineola, NY, 1989.
[31] B.L. Westcott, J.H. Enemark, in: E.I. Solomon, A.B.P. Lever (Eds.), Inorganic Electronic Structure and Spectroscopy, vol. II, John Wiley & Sons, New York, 1999, p. 403.
[32] D.R. Lang, J.A. Davis, L.G.F. Lopes, A.A. Ferro, L.C.G. Vasconcellos, D.W. Franco, E. Tfouni, A. Wieraszko, M.J. Clarke, Inorg. Chem. 39 (2000) 2294.
[33] J.N. Armor, Scheideg Ha, H. Taube, J. Am. Chem. Soc. 90 (1968) 5928.
[34] C.K. Poon, C.M. Che, J. Chem. Soc., Dalton Trans. (1981) 1336.
[35] E. Tfouni, K.Q. Ferreira, F.G. Doro, R.S. da Silva, Z.N. da Rocha, Coord. Chem. Rev. 249 (2005) 405.
[36] C. Creutz, M.H. Chou, Inorg. Chem. 26 (1987) 2995.
[37] (a) C. Creutz, M.D. Newton, N. Sutin, J. Photochem. Photobiol. A-Chem. 82 (1994) 47;
(b) A.M. Zwickel, C. Creutz, Inorg. Chem. 10 (1971) 2395.
[38] Y.G.K. Shin, B.S. Brunschwig, C. Creutz, M.D. Newton, N. Sutin, J. Phys. Chem. 100 (1996) 1104.
[39] (a) Y.K. Shin, B.S. Brunschwig, C. Creutz, N. Sutin, J. Phys. Chem. 100 (1996) 8157;
(b) L.D. Slep, J.A. Olabe, J. Am. Chem. Soc. 123 (2001) 7186.
[40] R.S. da Silva, M.T.P. Gambardella, R.H.A. Santos, B.E. Mann, E. Tfouni, Inorg. Chim. Acta 245 (1996) 215.
[41] R.S. da Silva, E. Tfouni, Inorg. Chem. 31 (1992) 3313.
[42] L.M. Baraldo, M.S. Bessega, G.E. Rigotti, J.A. Olabe, Inorg. Chem. 33 (1994) 5890.
[43] (a) D.A. Estrin, L.M. Baraldo, L.D. Slep, B.C. Barja, J.A. Olabe, L. Paglieri, G. Corongiu, Inorg. Chem. 35 (1996) 3897;
(b) M.C. Gonzalez-Lebrero, A.G. Turjanski, J.A. Olabe, D.A. Estrin, J. Mol. Model. 7 (2001) 201.
[44] (a) F. Bottomley, J.R. Crawford, J. Chem. Soc., Dalton Trans. (1972) 2145;
(b) P. Ford, D.F.P. Rudd, R. Gaunder, H. Taube, J. Am. Chem. Soc. 90 (1968) 1187.
[45] E. Tfouni, M. Krieger, B.R. McGarvey, D.W. Franco, Coord. Chem. Rev. 236 (2003) 57.
[46] V. Gutmann, Electrochim. Acta 21 (1976) 661.
[47] B.S. Brunschwig, C. Creutz, N. Sutin, Coord. Chem. Rev. 177 (1998) 61.